Fluid Mechanics Laboratory
Publication No. 71-7

THE EXCITATION MECHANISM OF THE NITROGEN FIRST POSITIVE AND FIRST NEGATIVE RADIATION AT HIGH TEMPERATURE

AD723530

Richard C. Flagan and John P. Appleton

April 1971

FLUID MECHANICS LABORATORY

DDC
RECEIVED
MAY 21 1971
C

DEPARTMENT OF MECHANICAL ENGINEERING
MASSACHUSETTS INSTITUTE OF TECHNOLOGY

Reproduced by
NATIONAL TECHNICAL
INFORMATION SERVICE
Springfield, Va. 22151

Unclassified
Security Classification

DOCUMENT CONTROL DATA - R&D

(Security classification of title, body of abstract and indexing annotation must be entered when the overall report is classified)

1. ORIGINATING ACTIVITY *(Corporate author)*
Massachusetts Institute of Technology
Cambridge, Massachusetts

2a. REPORT SECURITY CLASSIFICATION
Unclassified

2b. GROUP

3. REPORT TITLE
THE EXCITATION MECHANISM OF THE NITROGEN FIRST POSITIVE AND FIRST NEGATIVE RADIATION AT HIGH TEMPERATURE

4. DESCRIPTIVE NOTES *(Type of report and inclusive dates)*

5. AUTHOR(S) *(Last name, first name, initial)*
Flagan, Richard C. and Appleton, John P.

6. REPORT DATE
April 1971

7a. TOTAL NO. OF PAGES
31

7b. NO. OF REFS
39

8a. CONTRACT OR GRANT NO.
N00014-0204-0040

b. PROJECT NO.

c.

d.

9a. ORIGINATOR'S REPORT NUMBER(S)
Fluid Mechanics Laboratory
Publication No. 71-7

9b. OTHER REPORT NO(S) *(Any other numbers that may be assigned this report)*

10. AVAILABILITY/LIMITATION NOTICES
Distribution unlimited

11. SUPPLEMENTARY NOTES

12. SPONSORING MILITARY ACTIVITY
Advanced Research Projects Agency
Department of Defense and Office of
Naval Research, Washington, D.C.

13. ABSTRACT
The kinetic mechanisms responsible for the excitation of the first positive and first negative emission of nitrogen have been investigated in a re-examination of previously reported shock-tube measurements of the non-equilibrium radiation for these systems. The rate coefficients of the collisional quenching reactions:

$$N_2(A\ {}^3\Sigma_u^+) + N({}^4S) \xrightarrow{k_{-2}^{(N)}} N_2(X\ {}^1\Sigma_g^+) + N({}^4S)$$

and

$$N_2^+(B\ {}^2\Sigma_u^+) + N_2(X\ {}^1\Sigma_g^+) \xrightarrow{k_q^{(N_2)}} N_2^+(X\ {}^2\Sigma_g^+) \quad \text{or} \quad N_2^+(A\ {}^2\Pi_u) + N_2(X\ {}^1\Sigma_g^+)$$

were found to be given by the empirical expressions:

$$k_q^{(N)} = 1.9 \times 10^{-2}\ T^{-2.33} \qquad cm^3\ sec^{-1}$$

and

$$k_q^{(N_2)} = 1.9 \times 10^{-2}\ T^{-2.33} \qquad cm^3\ sec^{-1} \quad ,$$

respectively, over the approximate temperature range 6000° - 14000^oK.

DD FORM 1 JAN 64 1473

Unclassified
Security Classification

14. KEY WORDS	LINK A ROLE	LINK A WT	LINK B ROLE	LINK B WT	LINK C ROLE	LINK C WT
Nitrogen						
First positive radiation						
First negative radiation						
Chemical kinetics						
Electronic excitation						

INSTRUCTIONS

1. ORIGINATING ACTIVITY: Enter the name and address of the contractor, subcontractor, grantee, Department of Defense activity or other organization *(corporate author)* issuing the report.

2a. REPORT SECURITY CLASSIFICATION: Enter the overall security classification of the report. Indicate whether "Restricted Data" is included. Marking is to be in accordance with appropriate security regulations.

2b. GROUP: Automatic downgrading is specified in DoD Directive 5200.10 and Armed Forces Industrial Manual. Enter the group number. Also, when applicable, show that optional markings have been used for Group 3 and Group 4 as authorized.

3. REPORT TITLE: Enter the complete report title in all capital letters. Titles in all cases should be unclassified. If a meaningful title cannot be selected without classification, show title classification in all capitals in parenthesis immediately following the title.

4. DESCRIPTIVE NOTES: If appropriate, enter the type of report, e.g., interim, progress, summary, annual, or final. Give the inclusive dates when a specific reporting period is covered.

5. AUTHOR(S): Enter the name(s) of author(s) as shown on or in the report. Enter last name, first name, middle initial. If military, show rank and branch of service. The name of the principal author is an absolute minimum requirement.

6. REPORT DATE: Enter the date of the report as day, month, year; or month, year. If more than one date appears on the report, use date of publication.

7a. TOTAL NUMBER OF PAGES: The total page count should follow normal pagination procedures, i.e., enter the number of pages containing information.

7b. NUMBER OF REFERENCES: Enter the total number of references cited in the report.

8a. CONTRACT OR GRANT NUMBER: If appropriate, enter the applicable number of the contract or grant under which the report was written.

8b, 8c, & 8d. PROJECT NUMBER: Enter the appropriate military department identification, such as project number, subproject number, system numbers, task number, etc.

9a. ORIGINATOR'S REPORT NUMBER(S): Enter the official report number by which the document will be identified and controlled by the originating activity. This number must be unique to this report.

9b. OTHER REPORT NUMBER(S): If the report has been assigned any other report numbers *(either by the originator or by the sponsor)*, also enter this number(s).

10. AVAILABILITY/LIMITATION NOTICES: Enter any limitations on further dissemination of the report, other than those imposed by security classification, using standard statements such as:

(1) "Qualified requesters may obtain copies of this report from DDC."

(2) "Foreign announcement and dissemination of this report by DDC is not authorized."

(3) "U. S. Government agencies may obtain copies of this report directly from DDC. Other qualified DDC users shall request through _____."

(4) "U. S. military agencies may obtain copies of this report directly from DDC. Other qualified users shall request through _____."

(5) "All distribution of this report is controlled. Qualified DDC users shall request through _____."

If the report has been furnished to the Office of Technical Services, Department of Commerce, for sale to the public, indicate this fact and enter the price, if known.

11. SUPPLEMENTARY NOTES: Use for additional explanatory notes.

12. SPONSORING MILITARY ACTIVITY: Enter the name of the departmental project office or laboratory sponsoring *(paying for)* the research and development. Include address.

13. ABSTRACT: Enter an abstract giving a brief and factual summary of the document indicative of the report, even though it may also appear elsewhere in the body of the technical report. If additional space is required, a continuation sheet shall be attached.

It is highly desirable that the abstract of classified reports be unclassified. Each paragraph of the abstract shall end with an indication of the military security classification of the information in the paragraph, represented as *(TS)*, *(S)*, *(C)*, or *(U)*.

There is no limitation on the length of the abstract. However, the suggested length is from 150 to 225 words.

14. KEY WORDS: Key words are technically meaningful terms or short phrases that characterize a report and may be used as index entries for cataloging the report. Key words must be selected so that no security classification is required. Identifiers, such as equipment model designation, trade name, military project code name, geographic location, may be used as key words but will be followed by an indication of technical context. The assignment of links, rules, and weights is optional.

THE EXCITATION MECHANISM OF THE NITROGEN FIRST POSITIVE AND FIRST NEGATIVE RADIATION AT HIGH TEMPERATURE

by

Richard C. Flagan and John P. Appleton

Fluid Mechanics Laboratory

Department of Mechanical Engineering
Massachusetts Institute of Technology

This research was supported by the Advanced Research Projects Agency of the Department of Defense and monitored by the Office of Naval Research under Contract No. N00014-67-A-0204-0040 and ARPA Order No. 322.

This document has been approved for public release and sale; its distribution is unlimited.

March 1971

D D C
RECEIVED
MAY 21 1971
C

BLANK PAGE

The Excitation Mechanism of the Nitrogen First Positive and First Negative Radiation at High Temperature

Richard C. Flagan and John P. Appleton
Massachusetts Institute of Technology, Cambridge, Massachusetts

ABSTRACT

The kinetic mechanisms responsible for the excitation of the first positive and first negative emission of nitrogen have been investigated in a re-examination of previously reported shock-tube measurements of the non-equilibrium radiation for these systems. The rate coefficients of the collisional quenching reactions:

$$N_2(A\ ^3\Sigma_u^+) + N(^4S) \xrightarrow{k_{-2}^{(N)}} N_2(X\ ^1\Sigma_g^+) + N(^4S)$$

and

$$N_2^+(B\ ^2\Sigma_u^+) + N_2(X\ ^1\Sigma_g^+) \xrightarrow{k_q^{(N_2)}} N_2^+(X\ ^2\Sigma_g^+) \quad \text{or} \quad N_2^+(A\ ^2\Pi_u) + N_2(X\ ^1\Sigma_g^+)$$

were found to be given by the empirical expressions:

$$k_{-2}^{(N)} = 5.1 \times 10^{-3}\ T^{-2.23} \quad cm^3\ sec^{-1}$$

and

$$k_q^{(N_2)} = 1.9 \times 10^{-2}\ T^{-2.33} \quad cm^3\ sec^{-1}\ ,$$

respectively, over the approximate temperature range 6000° - $14000^\circ K$.

1. INTRODUCTION

The characteristic nonequilibrium radiation profiles which are observed in the relaxation region behind shock waves in nitrogen in the nominal wavelength intervals 6000-12000 Å and 3500-5000 Å are generally attributed to the first positive ($B\ ^3\Pi_g \rightarrow A\ ^3\Sigma^+_u$) and first negative ($B\ ^2\Sigma^+_u \rightarrow X\ ^2\Sigma^+_g$) band systems of N_2 and N_2^+, respectively. The characteristic features of this nonequilibrium emission have been investigated by several authors.[1-12] Qualitatively, the radiation rises rapidly to a peak immediately after the shock wave, the peak intensity being far in excess of that which would correspond to complete thermochemical equilibrium, and then decays in an exponential-like fashion to the ultimate equilibrium level. The emitting states of the two band systems, i.e., $N_2(B\ ^3\Pi_g)$ and $N_2^+(B\ ^2\Sigma^+_u)$, are separated by more than 10 e.V, and thus it is surprising that the times required to reach the peak intensity are quite comparable over a wide range of temperature,[12] typically 6000°-15000°K. This observation suggests common rate-limiting steps in the kinetic mechanisms which are responsible for populating both of the emitting states $N_2(B\ ^3\Pi_g)$ and $N_2^+(B\ ^2\Sigma^+_u)$.

In an attempt to examine the role of atomic nitrogen in shock-wave excitation mechanisms, Wray[11] fired shock waves into a nitrogen test gas which was already partially dissociated by means of a pulsed electrodeless discharge. Unfortunately, the initial atom concentrations in the test gas at the time when the shock waves passed the observation station were not accurately determined. The primary source of the inaccuracy appears to be that the low temperature recombination rate coefficient which

Wray used to estimate the atom concentration at the time of shock arrival was roughly a factor of ten greater than the more recent and generally accepted value.[13-15] However, on the basis of Wray's measurements,[11] it is possible to conclude that nitrogen atoms are very much more effective in promoting collisional excitation of nitrogen molecules to both the $N_2(B\ ^3\Pi_g)$ and $N_2^+(B\ ^2\Sigma_u^+)$ states than are the ground state molecules $N_2(^1\Sigma_g^+)$.

Recent improvements in our understanding of the gas phase dissociation and recombination kinetics of nitrogen, both experimentally[13-16] and theoretically,[17] prompted us to re-examine the role of atomic nitrogen in the excitation mechanisms which give rise to the first positive and first negative emission profiles observed behind shock waves. In this investigation we have used the measurements of the times to reach peak intensity and the radiation profile shapes which have been published in the literature,[1-11] together with some unpublished measurements, due to Wray,[12] of the times to reach peak intensity and the absolute emission intensities recorded in experiments where the test gas was not predissociated.

2. EXPERIMENTAL CONSIDERATIONS

2.1 Vibrational Relaxation

Figure 1 shows a plot of Wray's[12] measurements of the times, τ_{pk}, to reach peak intensity for both the $N_2(1+)$ and $N_2^+(1-)$ band systems as a function of temperature. All of the experiments were conducted using undiluted nitrogen at an initial pressure of 1 torr. The full line in Figure 1 shows the temperature variation of the characteristic vibrational relaxation time for ground state N_2 as measured by Millikan and White[18] and Appleton.[19] It is clear from this comparison that the nitrogen gas

was vibrationally relaxed well before the $N_2(1+)$ and $N_2^+(1-)$ radiation intensities had reached significant levels; thus the initial post-shock temperatures were calculated using the Rankine-Hugoniot equations, and the assumption that the translational, rotational, and vibrational energy modes of the N_2 were fully equilibrated. However, with increasing distance behind the shock front, the temperature and pressure will vary due to both the dissociation of N_2 molecules and to the development of the cold wall boundary layer which acts as a mass sink for the shocked test gas.

2.2 Boundary Layer Effects

The effects of the shock-tube boundary layer on the properties of the shocked test gas have been investigated by numerous authors.[20-26] For this reason we shall not dwell on the subject here. Mirel's[25,26] treatment, which allows corrections to the ideal shock-tube flow properties due to boundary layer development, is the most widely quoted. The primary effect of the boundary layer growth in kinetic studies performed in small bore shock tubes at low initial pressures is to decrease the time of flight of a fluid element which passes through the shock wave at a fixed position upstream of the observation station below that calculated on the basis of ideal shock tube theory. The corrections to the ideal flow properties are usually evaluated by assuming that at the observation station the shock and contact surface are travelling at the same speed; i.e., the mass leakage in the boundary layer which passes the contact surface is equal to the mass flux through the shock front. This condition was approximately satisfied in Wray's experiments. The mass continuity

equation for the inviscid flow external to the boundary layer may then be written in the form

$$\rho u = \rho_2 u_2 (1 - (x/\ell m)^{1/2}) \tag{2.1}$$

where $\rho_2 u_2 = \rho_1 U_s$, is the mass flux entering the shock wave, x is the distance measured downstream from the shock wave in shock-fixed coordinates, and ℓ_m is the maximum separation distance between the shock and the contact surface. Since it is assumed that the shock waves travel at the uniform velocity U_s, then

$$x = U_s t_L \tag{2.2}$$

where t_L is the laboratory observation time.

In order to analyze the chemically reacting flows obtained behind normal shock waves generated in a shock tube, we have developed a numerical computer program which uses a fourth-order Runga Kutta integration technique to solve the differential forms of the flow conservation equations together with the appropriate chemical rate equations. When viewed in shock-fixed coordinates, the flow is steady and is treated as being quasi-one-dimensional to account for the boundary layer mass loss as described by Equation 2.1. The independent variable used in the analysis is x which is related to the actual particle flight time t_f by the equation

$$dx/dt_f = u \ . \tag{2.3}$$

For a more detailed discussion of the calculation method, see the Appendix.

2.3 Emission Intensity Calculation

Having determined the temperature density and species concentration histories in the relaxation region, the spectral band intensities of the radiation were calculated using the smeared rotational line model

described by Keck, Camm, Kivel, and Wentink.[4] Thus the spectral intensity I_λ is given as

$$I_\lambda = 2hc^2(\Pi r_o)\ f[N]\ \langle\phi\rangle\ \lambda^{-5}(hc/kT)\ g''Q_r''Q_v''/g'Q_r'Q_v' \qquad (2.4)$$

where $r_o = e^2/mc^2$ is the classical electron radius, $f = |R(\bar{r})/ea_o|^2/3R_\infty\lambda$ is the absorption oscillator strength of the band system, and $|R(\bar{r})/ea_o|^2$ is the electronic transition moment dependent on the internuclear separation $\bar{r}$. The quantity ϕ is a dimensionless number of order unity which takes into account the details of the vibration-rotational spectrum, and the averaged quantity $\langle\phi\rangle$ is defined as

$$\langle\phi\rangle = \lambda^6 \int_{\lambda_1}^{\lambda_2} (\lambda')^{-6}\ R d\lambda' / \int_{\lambda_1}^{\lambda_2} R d\lambda' \qquad (2.5)$$

where R is the experimentally determined resolution function of the optical instruments used in the experiments.[11] [N'] is the upper state concentration, and g', Q_r', and Q_v' are the corresponding electronic degeneracy, rotational, and vibrational partition functions, respectively, which are evaluated by assuming that the translational, rotational, and vibrational temperatures are equal (the double primes identify the corresponding absorbing state quantities).

In the calculations which were carried out for the purpose of comparison with Wray's[12] absolute intensity measurements, values for the electronic transition moments were those given by Wurster[27] for the $N_2(1+)$ system, i.e., $|R(\bar{r})/ea_o|^2 = 0.096$, and by Buttrey and McChesney[28] for the $N_2^+(1-)$ system, i.e., $|R(\bar{r})/ea_o|^2 = 0.45$.

3. KINETIC MODELS AND COMPUTATIONS

3.1 Reaction Mechanism - $N_2(1+)$

The kinetic scheme which we have found to best describe the shock-tube measurements of the $N_2(1+)$ system is the following:

$$N_2(X\ ^1\Sigma_g^+) + M \xrightarrow{k_{+1}^{(M)}} 2N(^4S) + M \tag{1}$$

$$N_2(X\ ^1\Sigma_g^+) + N(^4S) \underset{k_{-2}^{(N)}}{\overset{k_{+2}^{(N)}}{\rightleftharpoons}} N_2(A\ ^3\Sigma_u^+) + N(^4S) \tag{2}$$

$$N_2(A\ ^3\Sigma_u^+) + M \xrightarrow{k_{+3}^{(M)}} 2N(^4S) + M \tag{3}$$

$$N_2(A\ ^3\Sigma_u^+) + M \underset{k_{-4}^{(M)}}{\overset{k_{+4}^{(M)}}{\rightleftharpoons}} N_2(B\ ^3\Pi_g) + M \tag{4}$$

$$N_2(B\ ^3\Pi_g) \xrightarrow{\tau_5^{-1}} N_2(A\ ^3\Sigma_u^+) + h\nu \tag{5}$$

Apart from our inclusion of reaction (3), the above set of reactions is the same as that previously proposed by Wray.[11] The overall rate of the dissociation of ground state N_2 behind shock waves has been measured over the temperature range 8000°-15000°K by Appleton, Steinberg, and Liquornik[16] for those cases where the collision partner M is either Ar, N_2, or N. Shui, Appleton, and Keck,[17] using the modified phase-space theory of reaction rates, have calculated the separate dissociation rate coefficients $k_{+1}^{(M)}$ and $k_{+3}^{(M)}$ for the case where the collision partner M is an argon atom. By assuming that the $N_2(A\ ^3\Sigma_u^+)$ state was in local thermodynamic equilibrium with the ground state, they were able to match both the absolute magnitude and temperature dependence of the measured dissociation rate coefficients quite well using what appears to be a fairly realistic form for the two-body interatomic potential V_{ArN}. On the basis of the results to be described later, it appears that for the

dissociation of N_2 diluted in an argon heat bath and at the temperatures of the shock-tube experiments, the assumption of local thermodynamic equilibrium is invalid. We shall also show that for the dissociation of pure N_2 at temperatures greater than about 8000°K, the A $^3\Sigma_u^+$ state concentration is well below that calculated on the basis of local thermodynamic equilibrium during the rise time of $N_2(1+)$ radiation, and thus the dissociation of both undiluted N_2 and of diluted N_2 at high temperatures behind shock waves proceeds primarily via the ground state, i.e., reaction (1). We have therefore used the experimentally derived dissociation rate coefficient $k_D^{(M)}$[16] for $k_{+1}^{(M)}$ but have additionally assumed that the ratio $k_{+3}^{(M)}/k_{+1}^{(M)}$ ($M = N_2$, Ar, N) is the same as that given by the phase-space theory calculations for M = Ar.[17] The ultimate justification for this assumption is provided by the results contained below; however, even on theoretical grounds we should anticipate this procedure to be approximately correct.*

In accord with Wray,[11] we have assumed reaction (4) to be sufficiently fast by comparison with any of the other reactions which serve to populate or depopulate either of the $N_2(A\ ^3\Sigma_u^+)$ or $N_2(B\ ^3\Pi_g)$ states that these two states may be assumed to be in local thermodynamic equilibrium with one another throughout the entire relaxation region. This assumption was subsequently justified by a numerical calculation in which we used our derived estimate for $k_{+2}^{(N)}$, the measured radiative lifetime of the B $^3\Pi_g$ state[39] ($\tau_5 = 7 \times 10^{-6}$ sec), and an estimate of the collisional

---

*The phase-space theory[17] assumes that the three-body interaction potential is given by the sum of two two-body potentials V_{N_2} and V_{NM}, where V_{N_2} is the ground state (X $^1\Sigma_g^+$) molecular potential for the calculation of $k_{+1}^{(M)}$, and the first excited state (A $^3\Sigma_u^+$) molecular potential for the calculation of $k_{+3}^{(M)}$. V_{NM} is simply the interatomic potential between an $N(^4S)$ atom and the third body M; it is independent of the ultimate state of the combined atoms.

quenching rate coefficient $k_{-4}^{(M)} = 6.2 \times 10^{-11}$ cm^3 sec^{-1} obtained at $T = 300^{\circ}$K. The rate of the dissociation reaction

$$N_2(B\ ^3\Pi_g) + M \rightarrow N(^4S) + N(^2D) + M$$

was shown theoretically[17] to be negligible by comparison with reaction (3) due to its increased endothermicity.

3.2 Calculations and Comparison with Experiment. $N_2(1+)$

Using the above values for $k_{+1}^{(M)}$, $k_{+3}^{(M)}$, and τ_5 (see Table I for a summary of the individual rate coefficients used) and the assumption that the A $^3\Sigma_u^+$ and B $^3\Pi_g$ states were maintained in local thermodynamic equilibrium, we were able to deduce the N-atom excitation rate coefficient, $k_{+2}^{(N)} = K_{e2}\ k_{-2}^{(N)}$, by matching our computed $N_2(1+)$ emission profiles with those observed experimentally. The matching procedure used was as follows: The rise of the emission intensity behind the shock wave was calculated to the peak using a guessed estimate for the value of the rate coefficient $k_{-2}^{(N)}$. The computed maximum intensity was then compared with Wray's[12] absolute measured value. By iteration on the value of the rate coefficient $k_{-2}^{(N)}$, the calculated peak intensity was brought into agreement with the experimental value. This matching procedure was employed at several shock speeds which spanned the full experimental range of conditions. The empirical rate coefficients thus obtained were correlated by the following expression:

$$k_{-2}^{(N)} = 5.1 \times 10^{-3}\ T^{-2.23}\ \text{cm}^3\ \text{sec}^{-1} \tag{3.1}$$

for the temperature range 6000°-14000°K. Figure 2 shows the comparison of our calculated peak intensities with Wray's[12] measurements.

In Figure 3 we have compared the values of $k_{-2}^{(N)}$ given by Equation 3.1 with those obtained by Wray[11] for the same temperature range, and with the room temperature rates determined by Young and St. John[31] and by Meyer, Setser and Stedman.[32] It is apparent that our estimate of $k_{-2}^{(N)}$ is more than an order of magnitude greater than Wray's estimate. We shall discuss the comparison shown in Figure 3 later in this report.

Additional tests of the kinetic model, reactions (1) - (5), and of the rate coefficients are provided by comparisons of the theoretically calculated times-to-peak intensity and the intensity profile shapes with the corresponding measurements; this information was not used in the matching procedure described above. Figure 4 presents a compilation of time-to-peak intensity data for the first positive emission obtained in shock-tube experiments using undiluted N_2,[4,9,12] N_2/Ar,[6] and N_2/Ne[10] mixtures. It is apparent that the calculated values of τ_{pk} for pure nitrogen agree very well with the experimental data. Similar good agreement is observed for the N_2/Ar mixtures, although the recorded time was not the actual time to peak but rather a characteristic time, τ'_{pk}, as shown in Figure 5. Since we anticipate that the dissociation rate coefficients, $k_{+1}^{(Ne)}$ and $k_{+3}^{(Ne)}$, for neon as the collision partner do not differ greatly from the argon rate coefficients, $k_{+1}^{(Ar)}$ and $k_{+3}^{(Ar)}$, the actual times to peak calculated for the N_2/Ar mixtures have also been plotted for comparison with the measurements made in N_2/Ne mixtures. Again the agreement between theory and experiment appears to be satisfactory.

A representative emission intensity profile shape is presented in Figure 5 for an observation made behind a shock wave in pure N_2. The shaded region represents the relative noise level of the oscilloscope

trace, and the full line represents the theoretically calculated profile. The similarity between the theoretical and experimental profiles which extends well into the region where thermochemical equilibrium is approached, further substantiates the kinetic model and the rate coefficients used.

The calculated concentration histories shown in Figure 6a and b for a shock wave in undiluted N_2 and in a 10 per cent N_2/Ar mixture, respectively, are helpful to our understanding of the radiation overshoots of the first positive emission. The pure nitrogen case, Figure 6a, corresponds to the radiation intensity profile of Figure 5. Due to the shock-tube boundary layer development, the ground-state molecule concentration is observed to increase slightly with time. The atom concentration remains small, reaching only 10 per cent of the ground-state molecule concentration at times well after the peak intensity is achieved, although, of course, for stronger shock waves the degree of dissociation increases rapidly, becoming about 25 per cent at the peak intensity for a post-shock temperature of about 14000°K.

The A $^3\Sigma_u^+$ state concentration at the intensity peak is about one-quarter of the local thermodynamic equilibrium value which is represented by the dashed curve in Figure 6a. This difference increases with increasing temperature so that the $N_2(A\ ^3\Sigma_u^+)$ concentration at peak intensity is less than one-tenth the equilibrium value at T_2 = 14000°K, whereas, at T_2 = 6000°K, it is greater than one-third of the equilibrium concentration. The reason for this relative behavior of the A $^3\Sigma_u^+$ concentration can be understood in terms of the expression which describes its steady-state variation. The steady state $N_2(A\ ^3\Sigma_u^+)$ concentration is achieved at about the time of the intensity maximum, and is given by:

$$(N_2^*) = k_{+2}^{(N)} (N_2) (N)/[k_{+3}^{(N_2)} (N_2) + k_{+3}^{(N)} (N) + k_{-2}^{(N)} (N)] \qquad (3.2)$$

where $N_2^* = N_2(A\ ^3\Sigma_u^+)$. At high temperatures where the atom concentration is large at the peak and the rate $k_{+3}^{(N)}$ is significantly greater than $k_{-2}^{(N)}$, the second term of the denominator dominates since the atom is much more efficient than the nitrogen molecule as a collision partner in the dissociation reactions. Thus Equation 3.2 may be approximated by

$$(N_2^*) = k_{+2}^{(N)} (N_2)/k_{+3}^{(N)} . \qquad (3.3)$$

At low temperatures ($T_2 < 6000^oK$) where, due to the exponential behavior of $k_{+3}^{(M)}$, the term $k_{-2}^{(N)}$ (N) at the peak intensity is much greater than $k_{+3}^{(N_2)}$ (N_2), the steady-state approximation reduces to the local thermodynamic equilibrium condition:

$$(N_2^*) = K_{e2} (N_2) . \qquad (3.4)$$

The experimental shock tube observations of the $N_2(1+)$ emission only approach these two extremes of the temperature range which satisfy either Equations 3.3 or 3.4. Over much of the experimental temperature range, the term $k_{+3}^{(N_2)}$ (N_2) is largest, but because the additional terms of the denominator are not wholly negligible, the steady-state concentration is only approximated by

$$(N_2^*) = k_{+2}^{(N)} (N)/k_{+3}^{(N_2)} . \qquad (3.5)$$

By tacitly assuming that during the intensity rise the N and N_2^* concentrations are populated according to the simplified rate equations

$$d(N)/dt = 2k_{+1}^{(N_2)} (N_2)^2 \qquad (3.6)$$

$$d(N_2^*)/dt = k_{+2}^{(N)} (N_2) (N) \tag{3.7}$$

and that the relaxation process is isothermal and the amount of dissociation is so small that the net rates of reactions (1) and (2) remain constant, we obtain by integration

$$(N) = 2k_{+1}^{(N_2)} (N_2)^2 t \tag{3.8}$$

and

$$(N_2^*) = k_{+2}^{(N)} k_{+1}^{(N_2)} (N_2)^3 t^2 . \tag{3.9}$$

We must remember that for pure nitrogen, particularly at high temperatures, the assumptions of constant N_2 concentration and temperature are valid only for times considerably shorter than the peak time. However, by approximating the population of the N_2^* state by Equation 3.9 until the steady-state concentration is reached, the important features of τ_{pk} become apparent. At the extreme high temperatures where the steady-state concentration is given by Equation 3.3, we find

$$(\tau_{pk} (N_2))^{-1} \sim (k_{+1}^{(N_2)} k_{+3}^{(N)})^{1/2} . \tag{3.10}$$

At the low temperature extreme where the assumptions of this simplified analysis are more closely satisfied, the local equailibrium concentration is reached at the peak, giving

$$(\tau_{pk}(N_2))^{-1} \sim (k_{+1}^{(N_2)} k_{-2}^{(N)})^{1/2} . \tag{3.11}$$

The steady-state concentration over the intermediate experimental temperature range is given approximately by Equation 3.5; thus

$$(\tau_{pk}(N_2))^{-1} \sim k_{+3}^{(N_2)} . \tag{3.12}$$

Since the assumptions leading to Equations 3.8 and 3.9 are only approximations at best, we may only reasonably expect the observed time to peak intensity to be correlated by a plot of log $[(\tau_{pk}\ (N_2))^{-1}]$ versus T^{-1}, as suggested by the form of Equations 3.10-3.12. Indeed, this expectation appears to be fully realized by the results shown in Figure 4. However, as we mentioned above, over most of the experimental temperature range, i.e., $T > 6000^{o}K$, the $N_2(A\ ^2\Sigma_u^+)$ concentration is much smaller than the corresponding equilibrium concentration, and thus the calculated times to peak are primarily determined by the dissociation reactions (1) and (3) and are much less dependent on reaction (2). Therefore, the good agreement between the calculated and measured times to peak as shown in Figure 4 must reflect the essential accuracy of the values which we have used for the dissociation rate coefficients $k_{+1}^{(M)}$ and $k_{+3}^{(M)}$ for $M = N_2$ and N.

Figure 6b shows that the $N_2(A\ ^3\Sigma_u^+)$ state concentration for a dilute N_2/Ar mixture remains well below the corresponding equilibrium concentration even beyond the intensity maximum. A similar analysis as that outlined above for the steady-state concentration of the $A\ ^3\Sigma_u^+$ state shows that in the limit of a dilute mixture, it is approximately given by

$$[N_2^*] = k_{+2}^{(N)}\ [N_2]\ [N]/k_{+3}^{(Ar)}\ [Ar] \tag{3.13}$$

over the experimental shock-tube temperature range. Using equations similar to Equations 3.8 and 3.9, we obtain

$$(\tau_{pk}[Ar])^{-1} \sim k_{+3}^{(Ar)}\ . \tag{3.14}$$

The same observation which was made for the case of undiluted N_2 is again valid; i.e., the good agreement between the calculated and measured

times-to-peak intesnity shown in Figure 4 for dilute mixtures substantiate the essential accuracy of the value for $k_{+3}^{(Ar)}$ which we have used in our calculations.

The accuracy of the rate coefficient $k_{-2}^{(N)}$ which we have determined here is, of course, dependent on the validity of the assumed kinetic scheme, the accuracy of the other rate coefficients which we have used, and the reliability of the flow model which has been used to take account of the shock-tube boundary layer effects. We have carried out exploratory calculations in which we altered the values of the rates of reactions (1) and (3) by factors of two; we also performed the calculations without making the boundary layer calculations. In this way we sought to establish the sensitivity of our derived values for $k_{-2}^{(N)}$ to the various assumptions. On this basis we conclude that the expression for $k_{-2}^{(N)}$ (Equation 3.1) is reliable to within a factor of about two over the temperature range 6000°-14000°K. Although there is no experimental evidence on which to base estimates of $k_{-2}^{(N)}$ within the temperature range 300°-6000°K, it is clear from the results shown in Figure 3 that a straight-line extrapolation would correlate both the room temperature measurements and our shock-tube estimates quite well.

Before leaving the subject of the $N_2(1+)$ emission, we shall briefly comment on two other reactions which have been suggested as being primary sources of the excited state $N_2(A\ ^3\Sigma_u^+)$. The first

$$2N_2(X\ ^1\Sigma_g^+) \rightarrow N_2(A\ ^3\Sigma_u^+) + N_2(X\ ^1\Sigma_g^+) \qquad (2a)$$

is spin forbidden, and although the N_2 ground state is by far the most abundant species immediately behind the shock waves, we were unable to

determine a rate coefficient for this reaction by our matching procedures which enabled us to correlate both the peak-intensity measurement and the time-to-peak intensity. In addition, it is to be noted that Noxon[33] concluded from observations made in high pressure nitrogen afterglow experiments that more than 10^9 collisions with ground state molecules are required to effect electronic de-excitation of the A $^3\Sigma_u^+$ state. Thus we believe that the above excitation reaction is too slow to be of importance in the shock wave experiments.

Smekhov and Losev[6] have suggested an alternative mechanism for the excitation of $N_2(A\ ^3\Sigma_u^+)$

$$N_2(X\ ^1\Sigma_g^+) + e^- \underset{k_{-2}^e}{\overset{k_{+2}^e}{\rightleftharpoons}} N_2(A\ ^3\Sigma_u^+) + e^- \qquad (2b)$$

where the electrons are generated by the associative ionization reaction to be discussed in the following section. Although the rate $k_{-2}^{(e)}$ may be much larger than $k_{-2}^{(N)}$, it is unlikely that the difference will be as great as the difference between the N and e^- concentrations except at very high temperatures. Using a recent estimate of the rate coefficient of reaction (2b),[34] i.e.,

$$k_{+2}^{(e)} = (5 \pm 2) \times 10^{-5}\ T^{0.8}\ e^{-80300/T}\ cm^3\ sec^{-1}$$

and our calculated values for the concentrations and temperatures at the $N_2(1+)$ emission peaks, we conclude that only as T_2 approaches 15000^oK does the contribution of reaction (2b) reach one-tenth of the rate of production of $N_2(A\ ^3\Sigma_u^+)$ by N_2 + N collisions.

3.3 Reaction Mechanism - $N_2^+(1-)$

The kinetic scheme which we have found to best describe the shock-tube measurements of the $N_2^+(1-)$ system follows directly from that proposed by Hammerling, Teare, and Kivel:[3]

$$N(^4S) + N(^4S) \underset{k_{-6}}{\overset{k_{+6}}{\rightleftharpoons}} N_2^+(X\ ^2\Sigma_g^+) + e^- \tag{6}$$

$$N_2(X\ ^1\Sigma_g^+) + N^+(^3P) \underset{k_{-7}}{\overset{k_{+7}}{\rightleftharpoons}} N_2^+(X\ ^2\Sigma_g^+) + N(^4S) \tag{7}$$

$$N_2^+(X\ ^2\Sigma_g^+) + M \underset{k_{-8}^{(M)}}{\overset{k_{+8}^{(M)}}{\rightleftharpoons}} N_2^+(A\ ^2\Pi_u) + M \tag{8}$$

$$N_2^+(A\ ^2\Pi_u) + M \underset{k_{-9}^{(M)}}{\overset{k_{+9}^{(M)}}{\rightleftharpoons}} N_2^+(B\ ^2\Sigma_u^+) + M \tag{9}$$

$$N_2^+(X\ ^2\Sigma_g^+) + M \underset{k_{-10}^{(M)}}{\overset{k_{+10}^{(M)}}{\rightleftharpoons}} N_2^+(B\ ^2\Sigma_u^+) + M \tag{10}$$

$$N_2^+(B\ ^2\Sigma_u^+) \xrightarrow{1/\tau_{11}} N_2^+(X\ ^2\Sigma_g^+) + h\nu \tag{11}$$

Dunn and Lordi[35] have recently estimated the associative ionization rate coefficient k_{-6} over the approximate temperature range 3500°-7200°K from measurements of the electron density decay rate obtained in a shock-tube wind tunnel nozzle. We have assumed that the expression which they give for k_{-6} can be extended to the higher temperatures which are of interest to us here.

Charge-exchange cross sections of the type associated with reaction (7) are known to be quite large; however, only crude estimates of the rate coefficients $k_{+7} = K_{e7}\, k_{-7}$ have been made; for example, Dunn and Lordi[35] suggest $k_{-7} = 1.3 \times 10^{13\pm1}\, T^{0.5}\ cm^3\ sec^{-1}$. An estimate of the rate coefficient for reaction (8), i.e., $k_{-8}^{(N_2)} = 10^{-9}\ cm^3\ sec^{-1}$, has been given by Bennett and Dalby[36] at $T = 300^{\circ}K$; we anticipate that k_{-8} would not exhibit a significantly stronger temperature dependence than was observed for $k_{-2}^{(N)}$, see Figure 3. Thus we carried out trial calculations based on the estimates of k_{-7} and k_{-8} given above and concluded that reactions (7) and (8) would achieve local equilibrium well within the time required for the $N_2^+(1-)$ radiation to reach its intensity maximum over the experimental shock-tube temperature range.

To proceed further, we assumed that not only were the $N_2^+(A\ ^2\Pi_u)$ and $N^+(^3P)$ states in local equilibrium with the ground states of the molecular ion, but in addition, we also assumed that the concentration of the $N_2^+(B\ ^2\Sigma_u^+)$ state was given by the steady-state approximation at all times; i.e.,

$$[N_2^+(B\ ^2\Sigma_u^+)] = \frac{k_{+9}^{(M)}\ [N_2^+(A\ ^2\Pi_u)]\ [M] + k_{10}^{(M)}[N_2^+(X\ ^2\Sigma_g^+)][M]}{k_{-9}^{(M)}[M] + k_{-10}^{(M)}\ [M] + \tau_{11}^{-1}}$$

$$= K_{e10}[N_2^+(X\ ^2\Sigma_g^+)]\ \left\{ \frac{k_q^{(M)}[M]}{k_q^{(M)}[M] + \tau_{11}^{-1}} \right\} \qquad (3.16)$$

where the radiative life-time of the $B\ ^2\Sigma_u^+$ state is $\tau_{11} = 6.58 \times 10^{-8}$ sec,[34] $K_{e10}[N_2^+(X\ ^2\Sigma_g^+)]$ is the equilibrium concentration of the $B\ ^2\Sigma_u^+$ state relative to the ground state of the ion, and $k_q^{(M)} = (k_{-9}^{(M)} + k_{-10}^{(M)})$ is the net collisional quenching rate of the $B\ ^2\Sigma_u^+$ state which we sought to determine.

3.4 Calculations and Comparison with Experiment: $N_2^+(1-)$

Radiation intensity profiles for the $N_2(1-)$ system were first computed for a range of conditions which spanned Wray's experimental shock-tube measurements. The dissociation kinetics of the N_2 were taken to be the same as those described previously, ionization was assumed to proceed via reaction (6), reactions (7) and (8) were assumed to be in local equilibrium, and the $N_2^+(B\ ^2\Sigma_u^+)$ state concentration was assumed to be given by the steady-state condition, Equation 3.16. By iteration on the value of $k_q^{(M)}$ at each temperature, it was a straightforward matter to match the calculated peak intensity with the absolute peak intensity measurements given by Wray.[12] In this way we deduced the following empirical expression for the net collisional quenching rate coefficient for the $B\ ^2\Sigma_u^+$ state:

$$k_q^{(N_2)} = 1.9 \times 10^{-2}\ T^{-2.33}\ cm^3\ sec^{-1}\ . \qquad (3.17)$$

The calculated peak intensities are compared with Wray's measurements in Figure 7, and a plot of $k_q^{(N_2)}$ (Equation 3.17) is shown in Figure 3 together with the estimates of the low temperature quenching rate coefficients determined by Brocklehurst[37] and Davidson and O'Neil[38] at $T = 300^oK$.

Figure 8 shows the comparison between measurements of the time required to reach the intensity maximum and our calculated estimates of these times. Since we have assumed that the $N_2^+(B\ ^2\Sigma_u^+)$ state concentration was given by the steady-state approximation, the calculated values of τ_{pk} are virtually independent of the rates of reactions (8) and (9). Rather, the good agreement between the experimental and theoretical values of τ_{pk} shown in Figure 8 reflect the essential accuracy of the dissociation rates and the

high temperature extrapolation of the rate for the associative ionization reaction, reaction (6), used in the calculations. Also shown in Figure 8 is the comparison between measurements of the characteristic time τ'_{pk} by Smekhov and Losev[6] (open circles) for 10 per cent N_2/Ar mixtures and computed values (dashed line) for which we assumed $k_q^{(Ar)} = k_q^{(N_2)}$. Again the comparison is seen to be quite good.

It is to be noted that the comparisons shown in Figure 8 are effected by plotting log $\{\tau_{pk}([N_2]\ [M])^{1/2}\}^{-1}$ versus T^{-1} rather than log $\{\tau_{pk}[M]\}^{-1}$ versus T^{-1} as in Figure 4 for the $N_2(1+)$ system. We shall now examine the reason for this method of comparison.

The species concentration profiles illustrated in Figures 6a and b show that the dominant ionic species up to the time of the intensity maximum is the ground state molecular ion. Furthermore, our calculations indicated that the peak intensity was achieved at about the time at which local equilibrium was approximately established for reaction (6); i.e.,

$$[N_2^+(X\ ^2\Sigma_g^+)] \simeq K_{e6}^{1/2}\ [N] \quad . \tag{3.18}$$

By assuming that during the major portion of the period τ_{pk}, the N_2 concentration did not change significantly and that the conditions behind the shock wave are isothermal, we obtain

$$\frac{d[N]}{dt} = k_{+1}^{(M)}[N_2]\ [M] \tag{3.19}$$

and

$$\frac{d[N_2^+]}{dt} = k_{+6}\ [N]^2 \tag{3.20}$$

for $t < \tau_{pk}$, and thus

$$[N_2^+] = 4k_{+1}^{(M)2}\ k_{+6}[N_2]^2\ [M]\ t^3/3\ . \tag{3.21}$$

By further assuming that Equation 3.21 is valid up to the point at which local equilibrium is approximately established for reaction (6), we then obtain

$$\{\tau_{pk}([N_2]\ [M])^{1/2}\}^{-1} \sim (k_{+1}^{(M)}\ k_{-6}\ K_{e6}^{1/2})^{1/2}\ . \tag{3.22}$$

This approximate result explains why τ_{pk} is primarily determined by the dissociation kinetics of N_2 and the rate of the associative ionization reaction, as previously suggested, and the reason for our choice of the form for the ordinate in Figure 8.

Figure 9 shows a comparison between a representative emission intensity profile (shaded region) for an observation behind a shock wave in an N_2/Ar mixture with the theoretically calculated profile given by the full line. The similarity between the theoretical and experimental profiles further substantiates the kinetic model and rate coefficients used.

As we observed for the case of the $N_2(1+)$ system, the reliability of our estimate for the collisional quenching rate of the $N_2^+(B\ ^2\Sigma_u^+)$ state is dependent on the validity of the model reaction scheme and on the accuracy of the other rate coefficients used in the calculations. For this model reaction scheme, we have adjusted various of the rates over their probable range of uncertainty to assess their relative importance in the overall calculation, and on this basis we suggest that our estimate of $k_q^{(M)}$ is probably accurate to within a factor of 2 or 3. Again, we point out that a linear extrapolation from our high temperature estimates of $k_q^{(M)}$ does appear to correlate with the low temperature measurements shown in Figure 3.

4. CONCLUSIONS

A computer program has been developed which allows calculations to be made of chemically reacting flows obtained behind normal shock waves produced in non-ideal shock tubes. With the aid of this program, non-equilibrium radiation intensity profiles for the $N_2(1+)$ and $N_2^+(1-)$ band systems have been calculated and compared with previously published[1-11] and unpublished[12] measurements. The model reaction schemes used in the calculations followed directly from those proposed in earlier studies,[3,11] and were found to yield good agreement with measurements of the absolute maximum intensity, time-to-peak intensity, and intensity profile shapes.

Rate coefficients for the collisional quenching of the $N_2(A\ ^3\Sigma_u^+)$ and $N_2^+(B\ ^2\Sigma_u^+)$ states via the reactions:

$$N_2(A\ ^3\Sigma_u^+) + N(^4S) \xrightarrow{k_{-2}^{(N)}} N_2(X\ ^1\Sigma_g^+) + N(^4S)$$

and

$$N_2^+(B\ ^2\Sigma_u^+) + N_2 \xrightarrow{k_q^{(N_2)}} N_2^+(A\ ^2\Pi_u) \quad \text{or} \quad N_2^+(X\ ^2\Sigma_g^+) + N_2$$

were deduced by matching the computed peak intensities with Wray's[12] measurements and were found to be correlated by the empirical expressions

$$k_{-2}^{(N)} = 5.1 \times 10^{-3}\ T^{-2.23}\ \ cm^3\ sec^{-1}$$

and

$$k_q^{(N_2)} = 1.9 \times 10^{-2}\ T^{-2.33}\ \ cm^3\ sec^{-1}$$

over the temperature range 6000°-$14000^\circ K$. The two rates so determined are observed to be of comparable magnitude, and both have a similar strong negative temperature dependence. The reasons for this similarity are not

clear, although it is to be noted from Figure 3 that these high temperature estimates of the rate coefficients extrapolate quite well to the corresponding low temperature measurements.

The good agreement between the computed and measured time-to-peak intensity and the general profile shapes for both the $N_2(1+)$ and $N_2^+(1-)$ systems was observed to result from the choice of the rate coefficients which describe the dissociation kinetics of nitrogen[16,17] and of the ionization mechanism.[35] In particular, it appears that Shui, Appleton, and Keck's[17] estimate of the ratio $k_{-3}^{(M)}/k_{-1}^{(M)}$, is substantiated, although it is apparent that their assumption that the $N_2(A\ ^3\Sigma_u^+)$ and ground states are in local equilibrium is invalid for dissociation behind shock waves at temperatures greater than about 6000°K. Since the contribution of the $A^3\Sigma_u^+$ state to the net dissociation rate is smaller than they suggested, it explains the lack of an observed induction time in the nitrogen dissociation measurements.[39] Finally, as a consequence of the comparisons presented here for the $N_2^+(1-)$ system, it appears that Dunn and Lordi's[35] expression for the rate coefficient, k_{+6}, of the associative-ionization reaction can be extended up to 14000°K.

5. APPENDIX

Nonequilibrium Shock-Tube Program

The flow properties behind normal shock waves in a reacting gas are determined by integration of the differential forms of the flow conservation equations for the steady quasi-one-dimensional flow as observed in a shock-fixed coordinate system:

$$\frac{d\rho}{dx} = -\frac{\rho_2 u_2}{2u}\frac{1}{(x\ell_m)^{1/2}} - \frac{\rho}{u}\frac{du}{dx} \tag{5.1}$$

$$\frac{dp}{dx} = - \rho u \frac{du}{dx} \tag{5.2}$$

$$\frac{dh}{dx} + u \frac{du}{dx} = 0 \ . \tag{5.3}$$

The effects of shock-tube boundary layer development on the inviscid flow are taken into account by the "mass sink" term which appears on the right-hand side of Equation 5.1. The subscript (2) refers to the conditions immediately behind the shock front.

By defining $\gamma_i = N_i/\rho$, where N_i is the number concentration of species i, h_i as the enthalpy per molecule of species i so that $h = \sum_i \gamma_i h_i$, and $Cp_i = dh_i/dT$, Equation 5.3 becomes

$$\sum_i h_i \frac{d\gamma_i}{dx} + \frac{dT}{dx} \sum_i \gamma_i Cp_i + u \frac{du}{dx} = 0 \ . \tag{5.4}$$

For a perfect gas

$$T = \frac{PM}{R\rho} \tag{5.5}$$

where the molecular weight M may be expressed as

$$M = \frac{N_o}{\sum_i \gamma_i} \ . \tag{5.6}$$

By differentiating Equation 5.5 with respect to x, we find

$$\frac{dT}{dx} = - \frac{P}{R\rho} \frac{M}{N_o} \sum_i \frac{d\gamma_i}{dx} + \frac{M}{R\rho} \frac{dP}{dx} - \frac{PM}{R\rho^2} \frac{dp}{dx} \ . \tag{5.7}$$

where

$$\frac{d\gamma_i}{dx} = \frac{1}{\rho u} \frac{dN_i}{dt} \tag{5.8}$$

and dN_i/dt is given by the usual kinetic rate equation. Equations 5.1 - 5.9 may now be combined to yield

$$\frac{du}{dx} = \frac{\dfrac{-\sum_i h_i \dfrac{dN_i}{dt}}{\rho u} + \dfrac{TM}{N_o \rho u}\left(\sum_i \gamma_i Cp_i\right)\left(\sum_i \dfrac{dN_i}{dt}\right) - \dfrac{T\left(\sum_i \gamma_i Cp_i\right)}{2(x\ell_m)^{1/2}\left(1 - (x\ell_m)^{1/2}\right)}}{u + \dfrac{T \sum_i \gamma_i Cp_i}{u}\left(1 - \dfrac{\rho u^2}{P}\right)} \qquad (5.9)$$

Equations 2.3, 5.2, 5.8, and 5.9 form the basis for a numerical integration which yields the complete nonequilibrium flow properties in the reaction zone behind the shock front.

Reaction	Rate Coefficient*	Reference
1. $N_2(X\ ^1\Sigma_g^+) + M \longrightarrow 2N(^4S) + M$	$k_{+1}^{(Ar)} = (2.3 \pm 0.2) \times 10^{-3}\ T^{-1.6} \exp(-D^{(N_2)}/kT)$	16
	$k_{+1}^{(N_2)} = (6.2 \pm 1.6) \times 10^{-3}\ T^{-1.6} \exp(-D^{(N_2)}/kT)$	16
	$k_{+1}^{(N)} = (2.7 \pm 1.0) \times 10^{-2}\ T^{-1.6} \exp(-D^{(N_2)}/kT)$	16
	$(D^{(N_2)}/k = 1.132 \times 10^5\ ^oK)$	
2. $N_2(A\ ^3\Sigma_u^+) + N(^4S) \longrightarrow N_2(X\ ^1\Sigma_g^+) + N(^4S)$	$k_{-2}^{(N)} = 5.1 \times 10^{-3}\ T^{-2.23}$	This work
3. $2N(^4S) + M \longrightarrow N_2(A\ ^3\Sigma_u^+) + M$	$k_{-3}^{(M)}/k_{-1}^{(M)} = 36T^{-0.36}$	17
4. $N_2(A\ ^3\Sigma_u^+) + M \rightleftharpoons N_2(B\ ^3\Pi_g) + M$	Local equilibrium	-
5. $N_2(B\ ^3\Pi_g) \longrightarrow N_2(A\ ^3\Sigma_u^+) + h\nu$	$\tau_5 = 7.0 \times 10^{-6}$ (sec)	29
6. $N_2^+(X\ ^2\Sigma_g^+) + e^- \longrightarrow 2N(^4S)$	$k_{-6} = (2.5 \pm 0.8) \times 10^{-2}\ T^{-1.5}$	35
7. $N_2^+(X\ ^2\Sigma_g^+) + N(^4S) \rightleftharpoons N_2(X\ ^1\Sigma_g^+) + N^+(^3P)$	Local equilibrium	-
8. $N_2^+(X\ ^2\Sigma_g^+) + M \rightleftharpoons N_2^+(A\ ^2\Pi_u) + M$	Local equilibrium	-
9. $N_2^+(B\ ^2\Sigma_u^+) + N_2 \longrightarrow N_2^+(A\ ^2\Pi_u) + N_2$	$k_q^{(N_2)} = (k_{-9}^{(N_2)} + k_{-10}^{(N_2)}) = 1.9 \times 10^{-2}\ T^{-2.33}$	This work
10. $N_2^+(B\ ^2\Sigma_u^+) + N_2 \longrightarrow N_2^+(X\ ^2\Sigma_g^+) + N_2$		
11. $N_2^+(B\ ^2\Sigma_u^+) \longrightarrow N_2^+(X\ ^2\Sigma_g^+) + h\nu$	$\tau_{11} = 6.58 \times 10^{-8}$ (sec.)	34

*Units: Species concentrations measured in particles per cm^3, time in sec., and temperature in ^oK.

TABLE I. Reaction Rate Coefficients Used in Calculation of Radiation Profiles

REFERENCES

1. R. A. Allen, J. C. Camm, and J. C. Keck, J. Quant. Spect. Rad. Transf. 1, 269 (1961).
2. R. A. Allen, J. C. Keck, and J. C. Camm, Phys. Fluids 5, 284 (1962).
3. P. Hammerling, J. D. Teare, and B. Kivel, Phys. Fluids 2, 422 (1959).
4. J. C. Keck, J. C. Camm, B. Kivel, and T. Wentink, Jr., Ann. Phys. 7, 1 (1959).
5. S. A. Losev and G. D. Smekhov, High Temperature 2, 889 (1965).
6. G. D. Smekhov and S. A. Losev, High Temperature 6, 369 (1968).
7. K. L. Wray and T. J. Connolly, J. Quant. Spect. Rad. Transf. 5, 111 (1965).
8. R. A. Allen, J. Quant. Spect. Rad. Transf. 5, 511 (1965).
9. W. H. Wurster and P. V. Marrone, J. Quant. Spect. Rad. Transf. 7, 591 (1967).
10. P. V. Marrone, W. H. Wurster and J. E. Stratton, "Shock-Tube Studies of N^+ and O^+ Recombination Radiation in the Vacuum Ultraviolet," Cornell Aero. Lab. Rept. AG-1729-A-7, June 1968.
11. K. L. Wray, J. Chem. Phys. 44, 623 (1966).
12. We are grateful to Dr. K. L. Wray of Avco-Everett Research Lab for supplying us with his unpublished measurements of the time to reach peak intensity and the absolute maximum intensity.
13. I. M. Cambell and B. A. Thrush, Proc. Roy. Soc. A296, 201 (1967).
14. M. A. A. Clyne and D. H. Stedman, J. Chem. Phys. 49, 425 (1968).
15. F. Kaufman, Ann. Rev. Phys. Chem. 20, 45 (1969).
16. J. P. Appleton, M. Steinberg, and D. J. Liquornik, J. Chem. Phys. 48, 599 (1968).

17. V. H. Shui, J. P. Appleton, and J. C. Keck, J. Chem. Phys. 53, 2547 (1970).

18. R. C. Millikan and D. R. White, J. Chem. Phys. 39, 3209 (1963).

19. J. P. Appleton, J. Chem. Phys. 47, 3231 (1967).

20. R. E. Duff, Phys. Fluids 2, 207 (1959).

21. A. Roshko, Phys. Fluids 3, 835 (1960).

22. W. J. Hooker, Phys. Fluids 4, 1451 (1961).

23. H. Mirels, Phys. Fluids 6, 1201 (1963).

24. P. J. Musgrove and J. P. Appleton, Appl. Sci. Res. 18, 116 (1967).

25. H. Mirels, Phys. Fluids 9, 1265 (1966).

26. H. Mirels, Phys. Fluids 9, 1907 (1966).

27. W. H. Wurster. Cornell Aero. Labs Rept. No. QM-1626-A-3, Jan. 1962.

28. D. E. Buttrey and H. R. McChesney, "Analysis of Emission Intensity Data for Shock-Heated N_2, O_2, NO, and Air," Air Force Weapons Laboratory Technical Rept. No. AFWL-TR-69-29, Dec. 1969.

29. M. Jeunehomme, J. Chem. Phys. 45, 1805 (1966).

30. W. Brennan and E. C. Shane, Chem. Phys. Lett. 2, 143 (1968).

31. R. A. Young and G. A. St. John, J. Chem. Phys. 48, 895 (1968).

32. J. A. Meyer, D. W. Setser, and D. H. Stedman, J. Phys. Chem. 74, 2238 (1970).

33. J. F. Noxon, J. Chem. Phys. 36, 926 (1962).

34. F. R. Gilmore, E. Bauer, and J. W. McGowan, J. Quant. Spect. Rad. Transf. 9, 157 (1969).

35. M. G. Dunn and J. A. Lordi, "Measurement of $N_2^+ + e^-$ Dissociative Recombination in Expanding Nitrogen Flows," Cornell Aero. Lab. Rept. AI-2187-A-13, April 1969.

36. R. G. Bennet and F. W. Dalby, J. Chem. Phys. 31, 435 (1959).

37. B. Brocklehurst, Trans. Faraday Soc. 60, 2151 (1964).

38. G. Davidson and R. O'Neil, J. Chem. Phys. 41, 3946 (1964).

39. J. P. Appleton, M. Steinberg, and D. J. Liquornik, J. Chem. Phys. 52, 2205 (1970).

FIGURE CAPTIONS

Fig. 1 Comparison of measured times-to-peak intensity due to Wray[12] (P_1 = 1 Torr) and the characteristic vibrational relaxation time, τ_v.[18-19] ●, $N_2(1+)$; ○, $N_2^+(1-)$; full line, τ_v.

Fig. 2 Comparison of measured and calculated peak intensities of the $N_2(1+)$ emission. ●, Wray;[12] full lines, this work.

Fig. 3 Comparison of collisional quenching rates. $k_{-2}^{(N)}$: ●, Young and St. John;[31] ▲, Meyer, Setser, and Stedman;[32] full lines, this work and Wray[11] as indicated. $k_q^{(N_2)}$: ○, Brocklehurst;[37] △, Davidson and O'Neil;[38] broken line, this work.

Fig. 4 Comparison of measured and calculated time-to-peak intensity of the first positive system. Wray:[12] ●, 100% N_2, P_1 = 1 Torr; Wurster and Marrone:[9] ▲, 100% N_2, P_1 = 1-5 Torr; Keck, Camm, Kivel, and Wentink:[4] ◇, 100% N_2, P_1 = 1 Torr; ◆, P_1 = 3 Torr; ◐, P_1 = 10 Torr; Smekhov and Losev:[7] ○, 10% N_2 + 90% Ar, P_1 = 2-10 Torr; Marrone, Wurster, and Stratton:[10] ⬢, 10% N_2 + 90% Ne, P_1 = 2 Torr; ⧫, 7% N_2 + 93% Ne, P_1 = 2 Torr; △, 3% N_2 + 97% Ne, P_1 = 2 Torr; ⬡, 3% N_2 + 97% Ne, P_1 = 4 Torr; ▽, 0.5% N_2 + 99.5% Ne, P_1 = 4 Torr; ◊, 3% N_2 + 97% Ne, P_1 = 6 Torr; ▼, 0.5% N_2 + 99.5% Ne, P_1 = 6 Torr.

———, calculated τ_{pk}, 100% N_2, P_1 = 1 Torr; - - - - - - , calculated τ'_{pk}, 10% N_2 + 90% Ar, P_1 = 6 Torr; ——— – ——— , calculated τ_{pk}, 10% N_2 + 90% Ar, P_1 = 6 Torr.

Fig. 5 Comparison of theoretically calculated $N_2(1+)$ emission profile (full line) with experimental profile of Wray.[11] 100% N_2, U_2 = 4.56 mm/μsec, P_1 = 1 Torr, T_2 = 8210 °K.

Fig. 6 Computed concentration histories. _____ , calculated; - - - - - - , local thermodynamic equilibrium; _____ - _____ , temperature.

a) Wray[11] profile: 100% N_2, U_s = 4.56 mm/μsec, P_1 = 1 Torr, T_2 = 8210 °K.

b) Smekhov and Losev[6] profile: 10% N_2 + 90% Ar, U_s = 3.35 mm/μsec, P_1 = 6 Torr, T_2 = 9550 °K.

Fig. 7 Comparison of measured and calculated peak intensities of the $N_2^+(1-)$ emission. ●, Wray;[12] full line, this work.

Fig. 8 Comparison of measured and calculated time-to-peak intensity of the first negative system. Wray:[12] ●, 100% N_2, P_1 = 1 Torr; Smekhov and Losev:[6] O, 10% N_2 + 90% Ar, P_1 = 1-10 Torr. Full line: τ_{pk}, 100% N_2; broken line: τ_{pk}, 10% N_2 + 90% Ar.

Fig. 9 Comparison of theoretically calculated $N_2^+(1-)$ emission profile (full line) with experimental profile (shaded region) due to Smekhov and Losev:[6] 10% N_2 + 90% Ar, U_s = 3.35 mm/μsec, P_1 = 6 Torr, T_2 = 9550 °K.

BLANK PAGE

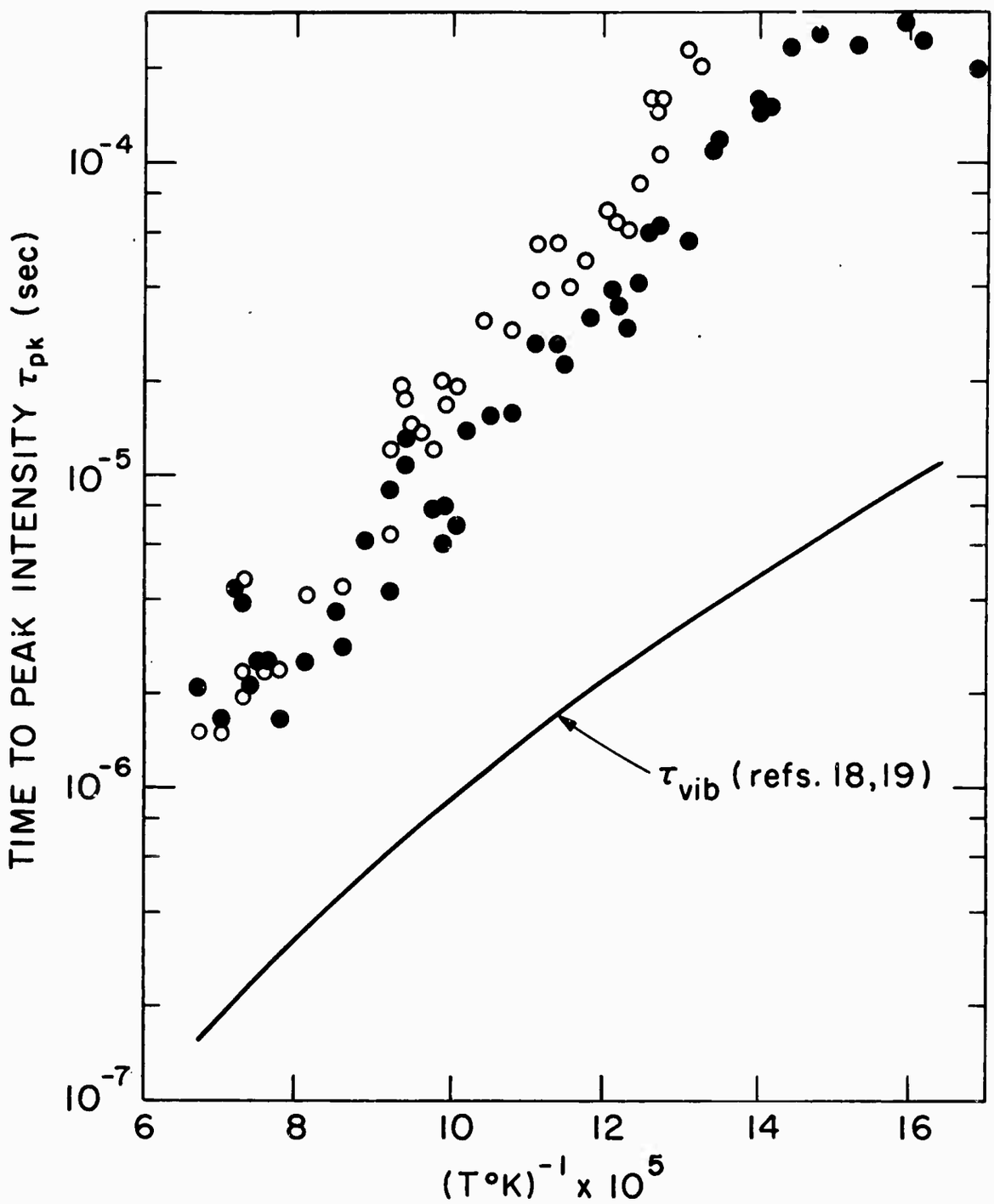
TIME TO PEAK INTENSITY τ_{pk} (sec)
10^{-4}
10^{-5}
10^{-6}
10^{-7}
6
8
10
12
14
16
$(T°K)^{-1} \times 10^5$
τ_{vib} (refs. 18,19)

FIGURE 1

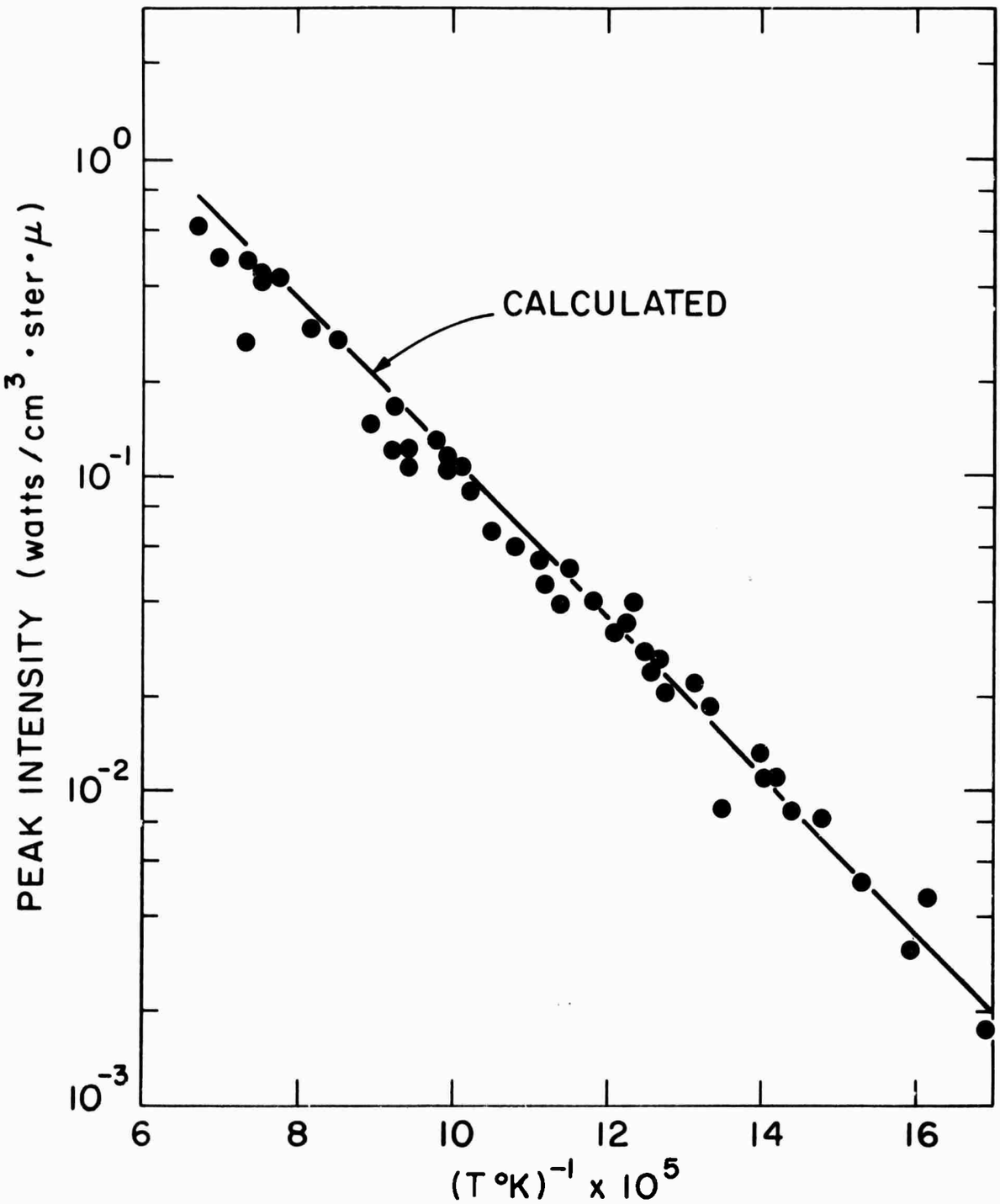
PEAK INTENSITY (watts/cm^3 • ster • μ)
10^0
10^{-1}
10^{-2}
10^{-3}
CALCULATED
6
8
10
12
14
16
$(T\,°K)^{-1} \times 10^5$

FIGURE 2

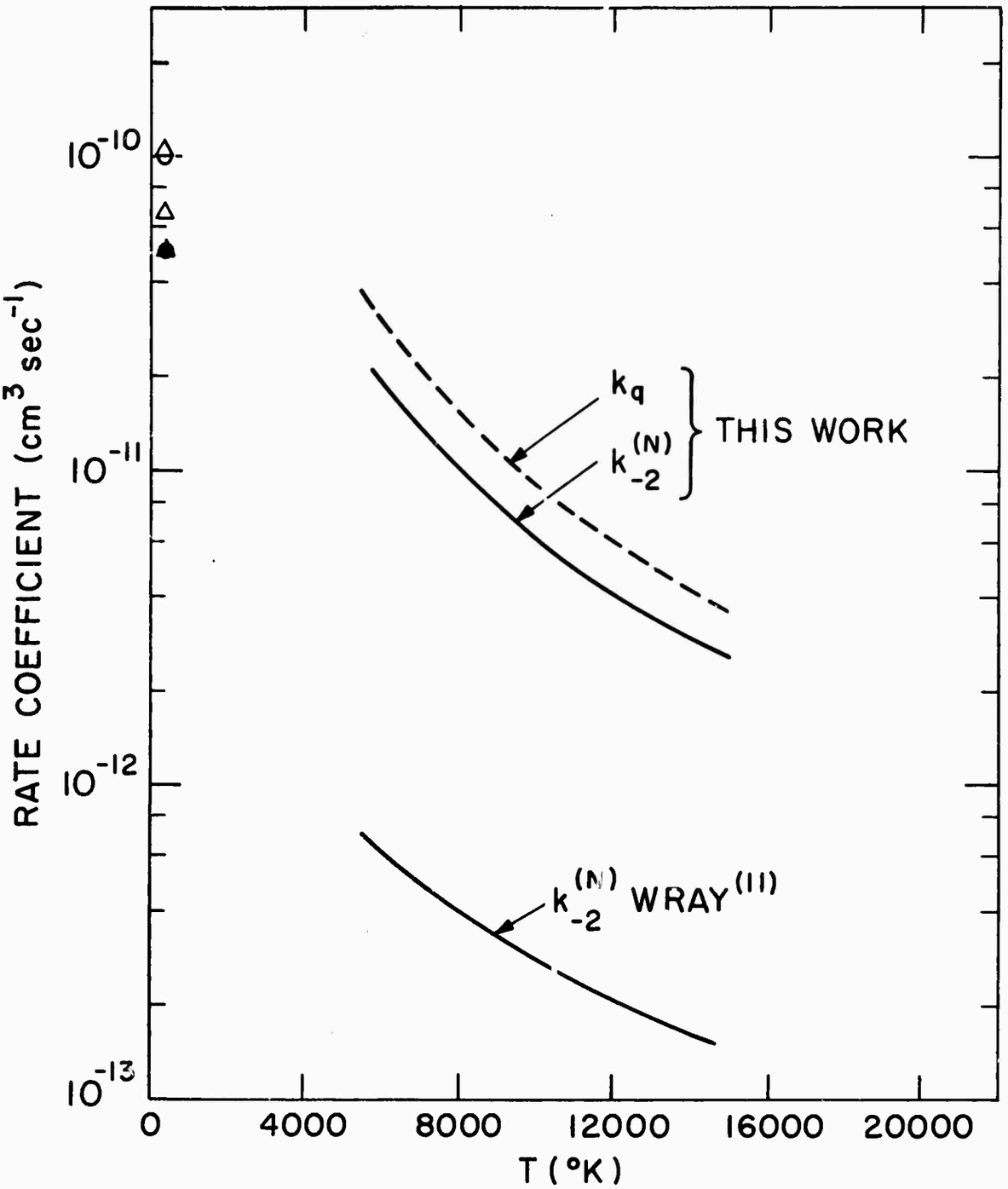
RATE COEFFICIENT (cm^3 sec^{-1})
10^{-10}
10^{-11}
10^{-12}
10^{-13}
0
4000
8000
12000
16000
20000
T (°K)
k_q
$k_{-2}^{(N)}$
THIS WORK
$k_{-2}^{(N)}$ WRAY[11]

FIGURE 3

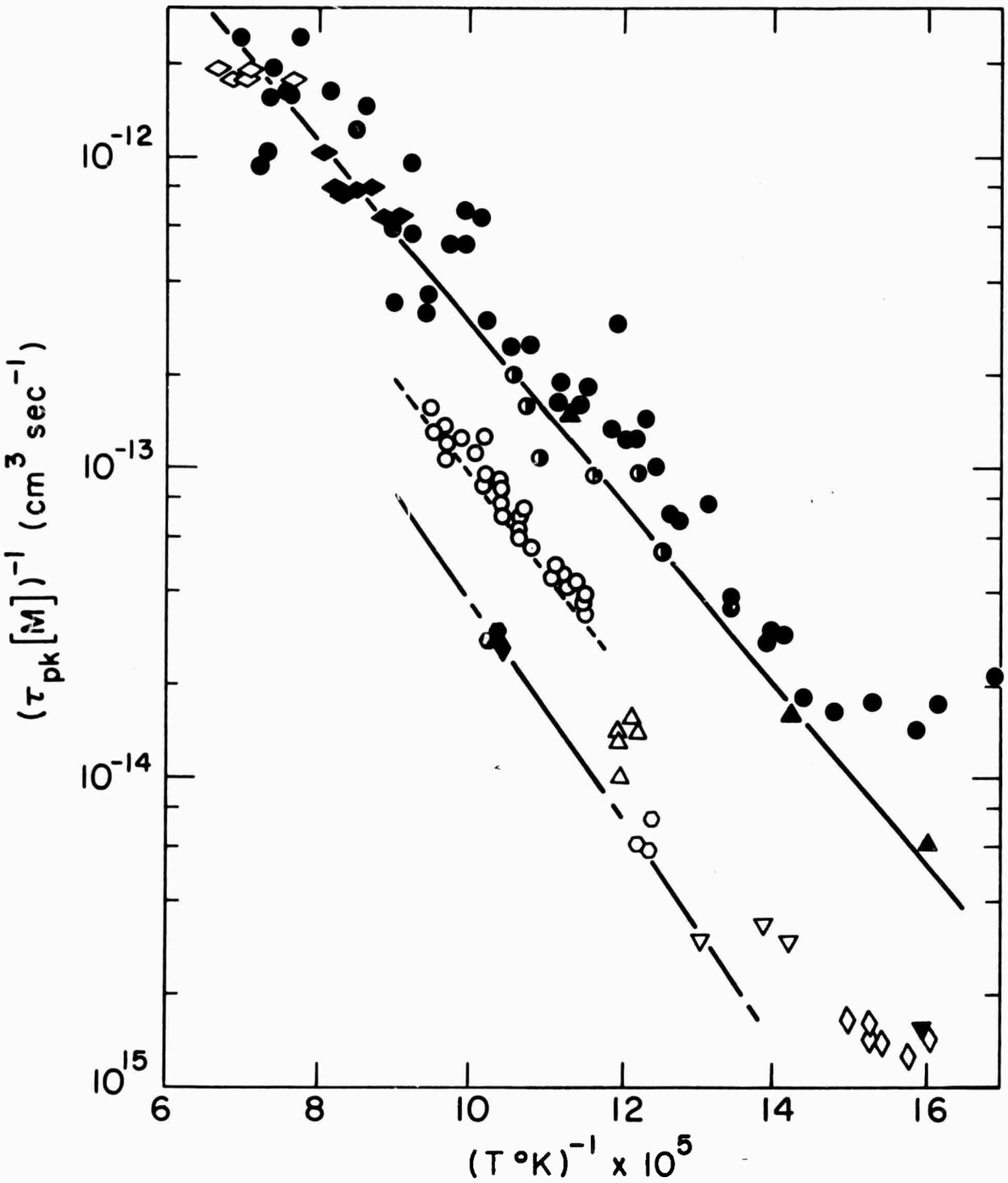
10^{-12}
10^{-13}
10^{-14}
10^{15}
$(\tau_{pk}[M])^{-1}$ $(cm^3\ sec^{-1})$
6
8
10
12
14
16
$(T\ °K)^{-1} \times 10^5$

FIGURE 4

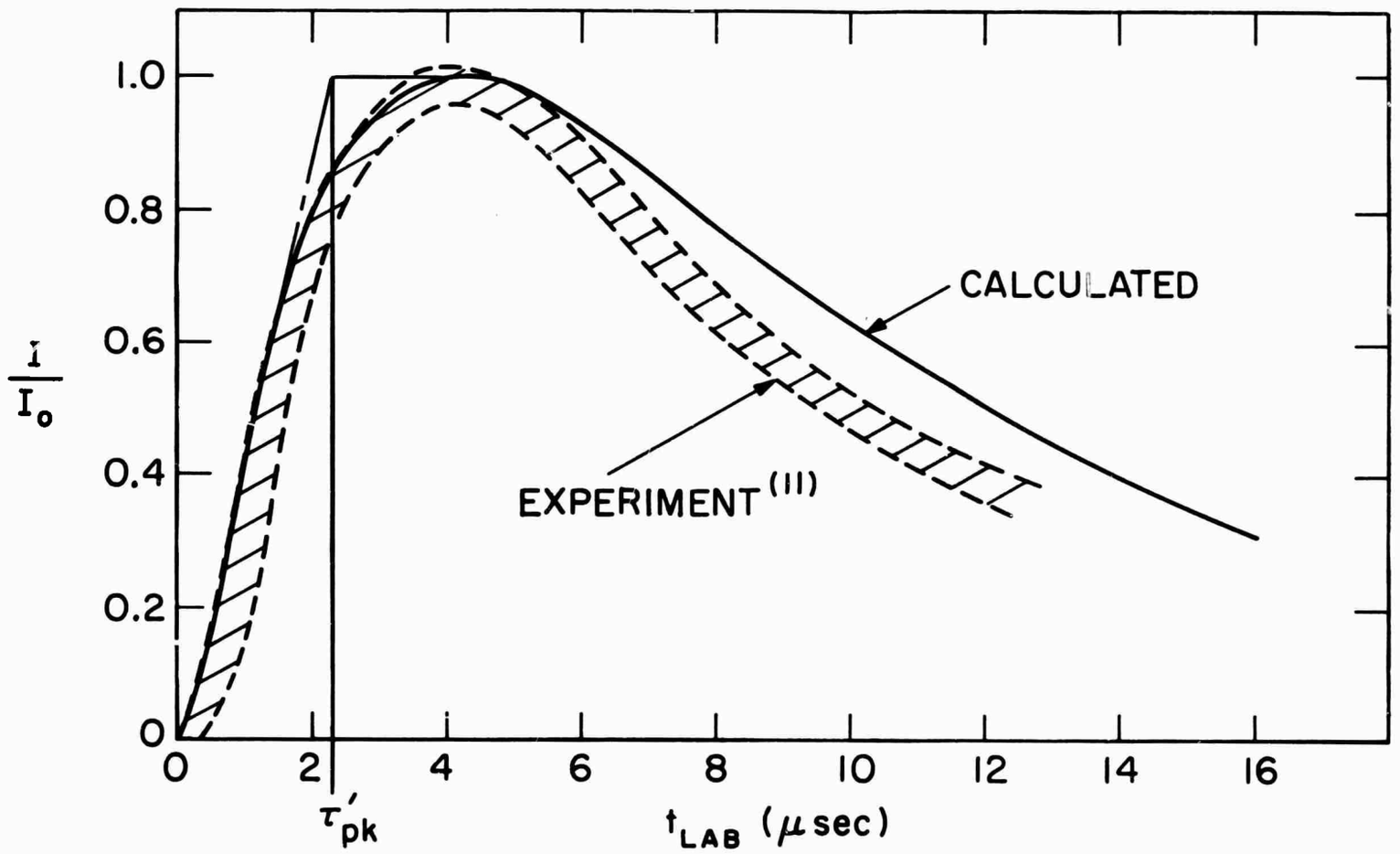
1.0
0.8
0.6
0.4
0.2
0
$\frac{I}{I_o}$
0
2
4
6
8
10
12
14
16
τ'_{pk}
t_{LAB} (μsec)
CALCULATED
EXPERIMENT (11)

FIGURE 5

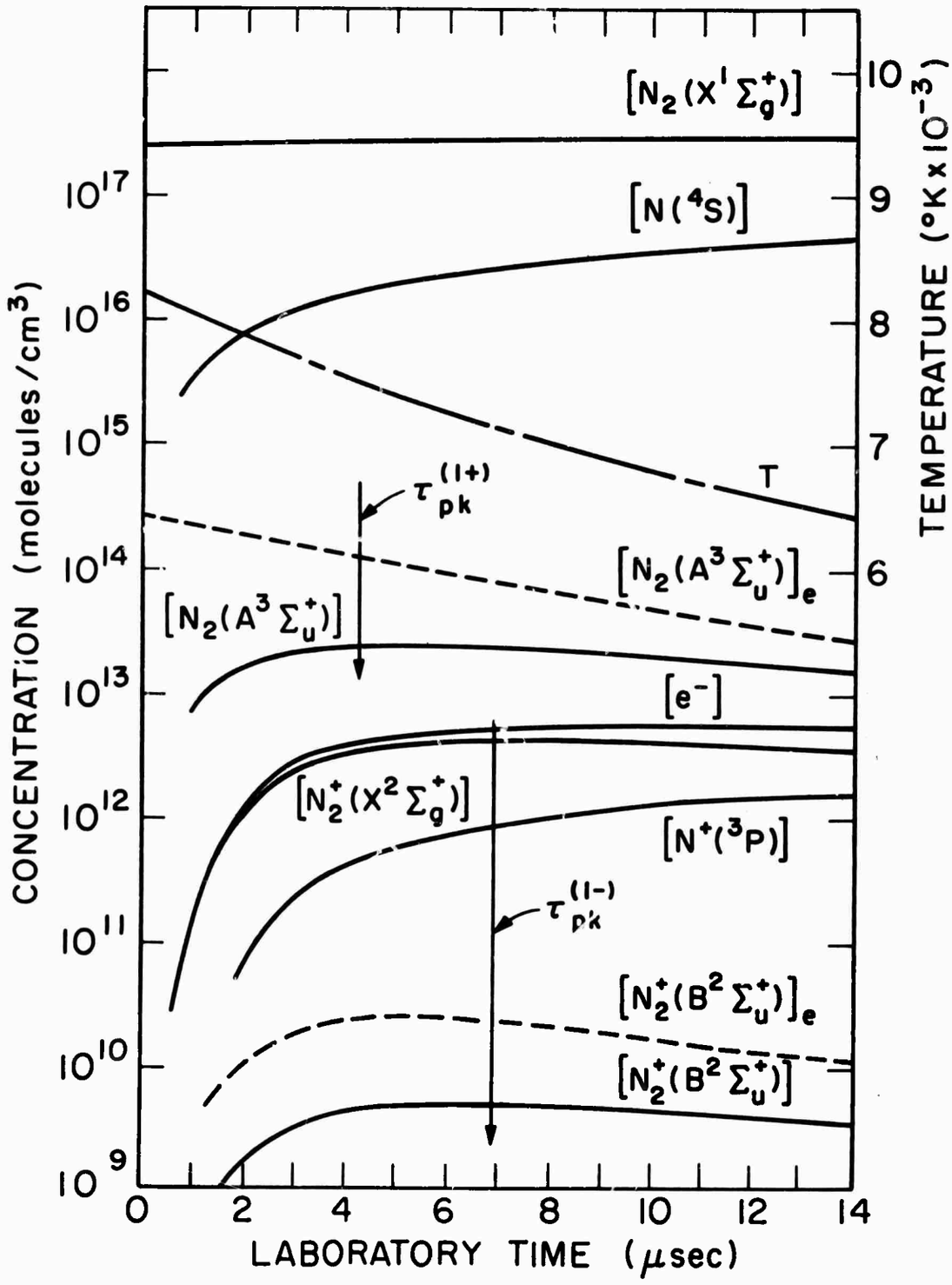
[N2(X1Σg+)]
[N(4S)]
T
[N2(A3Σu+)]e
[N2(A3Σu+)]
[e−]
[N2+(X2Σg+)]
[N+(3P)]
[N2+(B2Σu+)]e
[N2+(B2Σu+)]
τpk(1+)
τpk(1−)
CONCENTRATION (molecules/cm3)
TEMPERATURE (°K x 10−3)
LABORATORY TIME (μsec)
10^17
10^16
10^15
10^14
10^13
10^12
10^11
10^10
10^9
10
9
8
7
6
0
2
4
6
8
10
12
14

FIGURE 6(a)

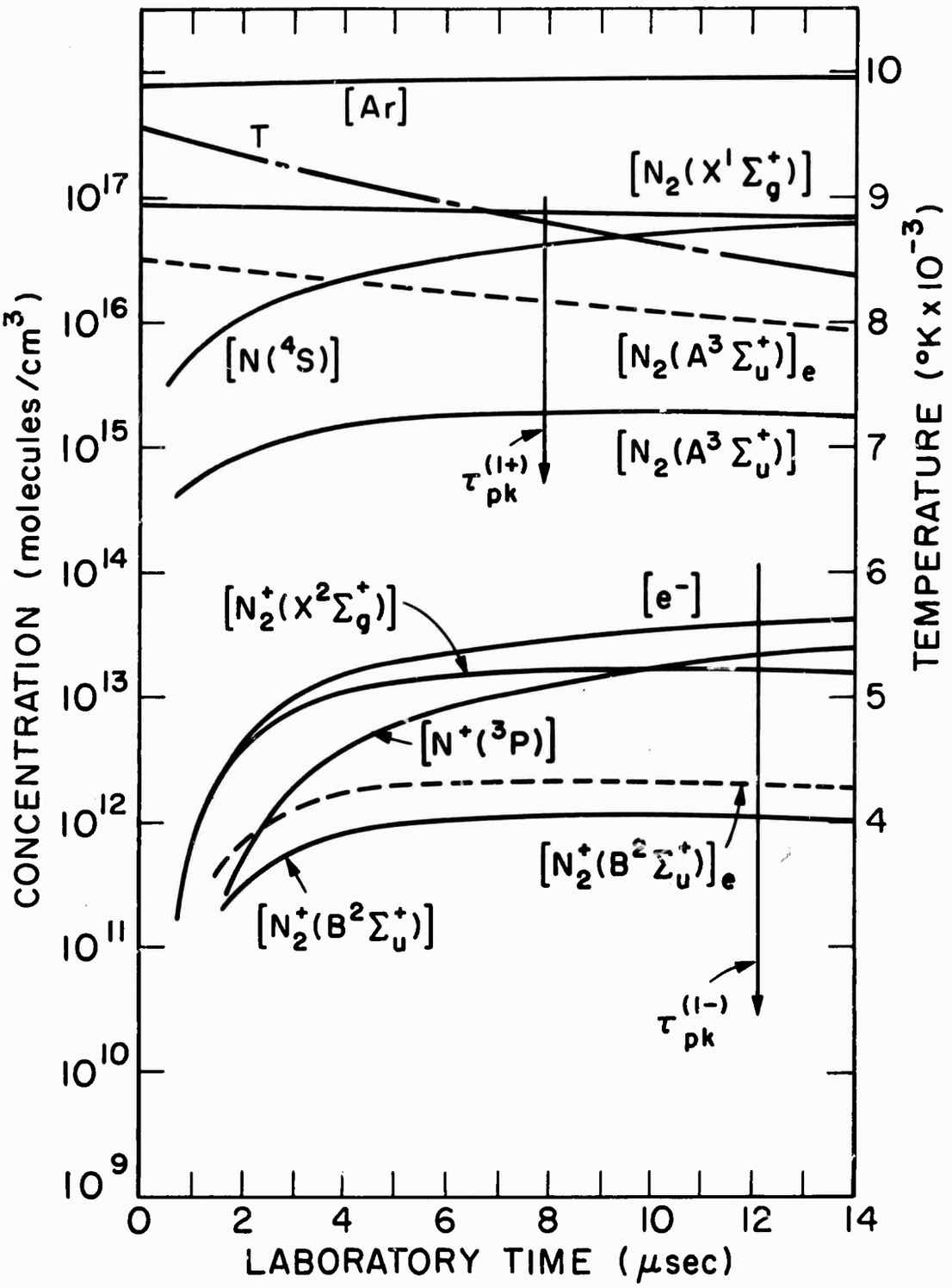
[Ar]
T
$[N_2(X^1\Sigma_g^+)]$
$[N(^4S)]$
$[N_2(A^3\Sigma_u^+)]_e$
$[N_2(A^3\Sigma_u^+)]$
$\tau_{pk}^{(1+)}$
$[N_2^+(X^2\Sigma_g^+)]$
$[e^-]$
$[N^+(^3P)]$
$[N_2^+(B^2\Sigma_u^+)]_e$
$[N_2^+(B^2\Sigma_u^+)]$
$\tau_{pk}^{(1-)}$
CONCENTRATION (molecules/cm^3)
TEMPERATURE (°K x 10^{-3})
LABORATORY TIME (μsec)
10^{17}
10^{16}
10^{15}
10^{14}
10^{13}
10^{12}
10^{11}
10^{10}
10^{9}
0
2
4
6
8
10
12
14
10
9
8
7
6
5
4

FIGURE 6 (b)

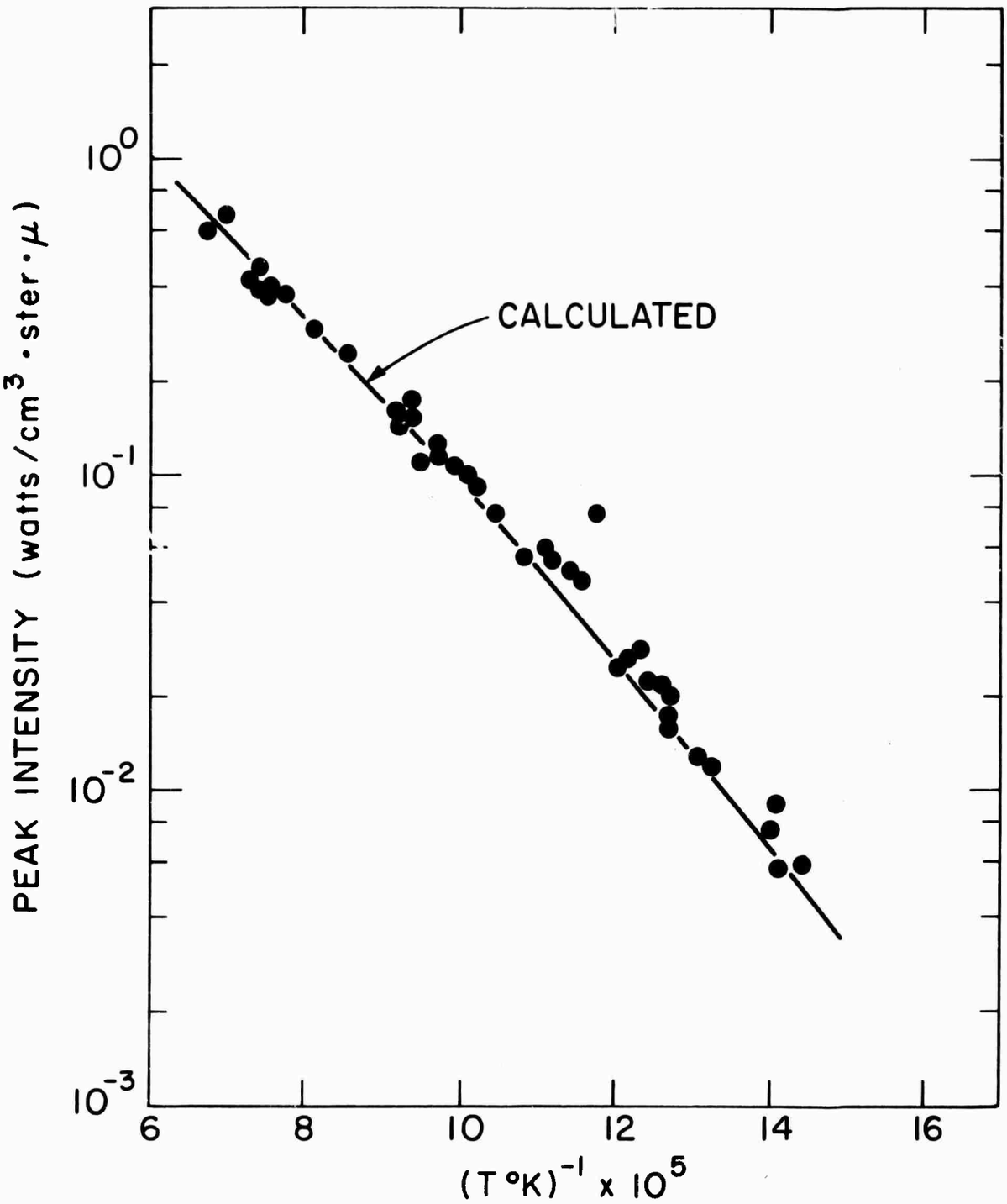
PEAK INTENSITY (watts/cm^3 • ster • μ)
10^0
10^{-1}
10^{-2}
10^{-3}
CALCULATED
6
8
10
12
14
16
$(T\,°K)^{-1} \times 10^5$

FIGURE 7

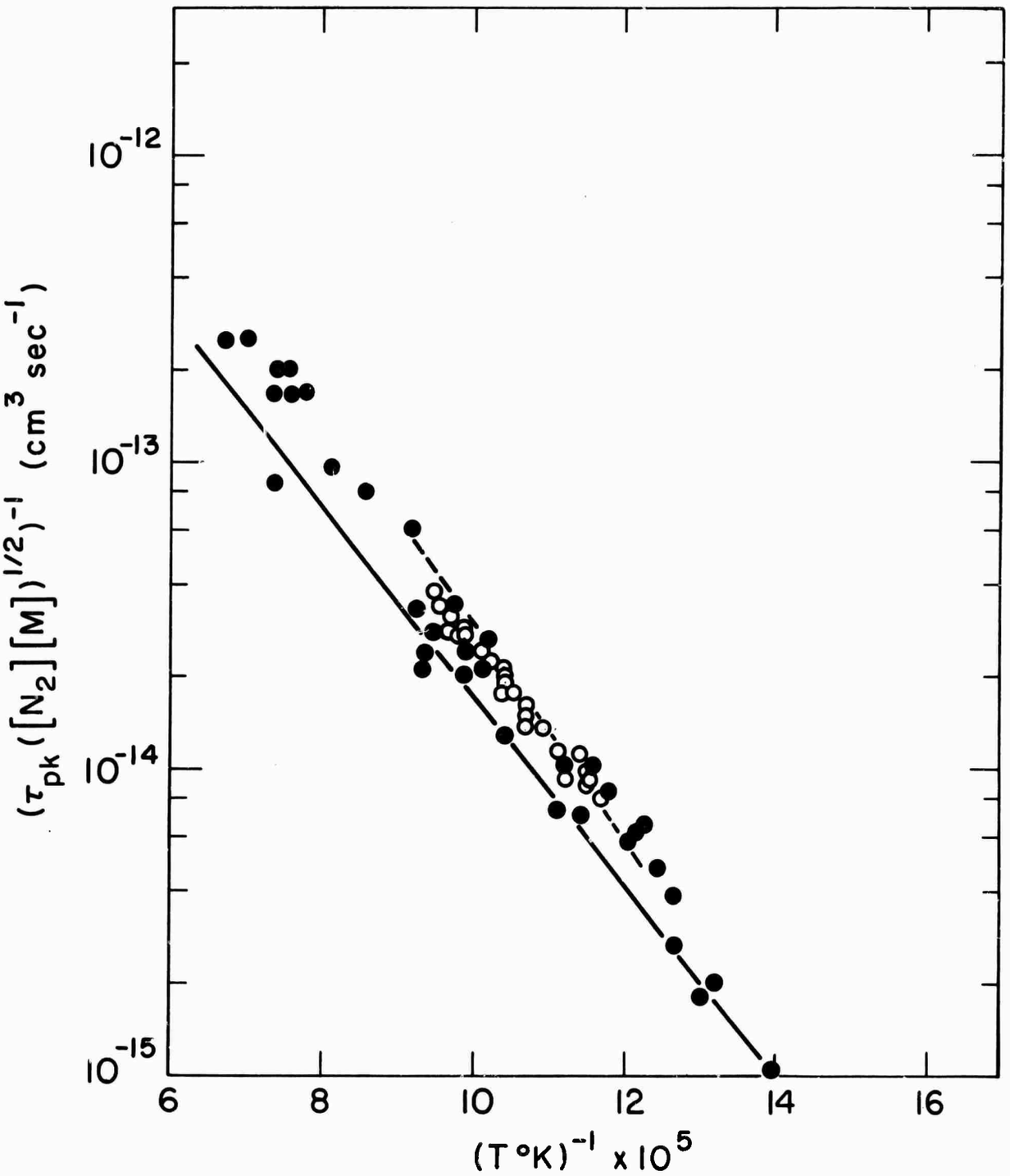
10^{-12}
10^{-13}
10^{-14}
10^{-15}
$(\tau_{pk}([N_2][M])^{1/2})^{-1}$ $(cm^3 sec^{-1})$
6
8
10
12
14
16
$(T\,°K)^{-1} \times 10^5$

FIGURE 8

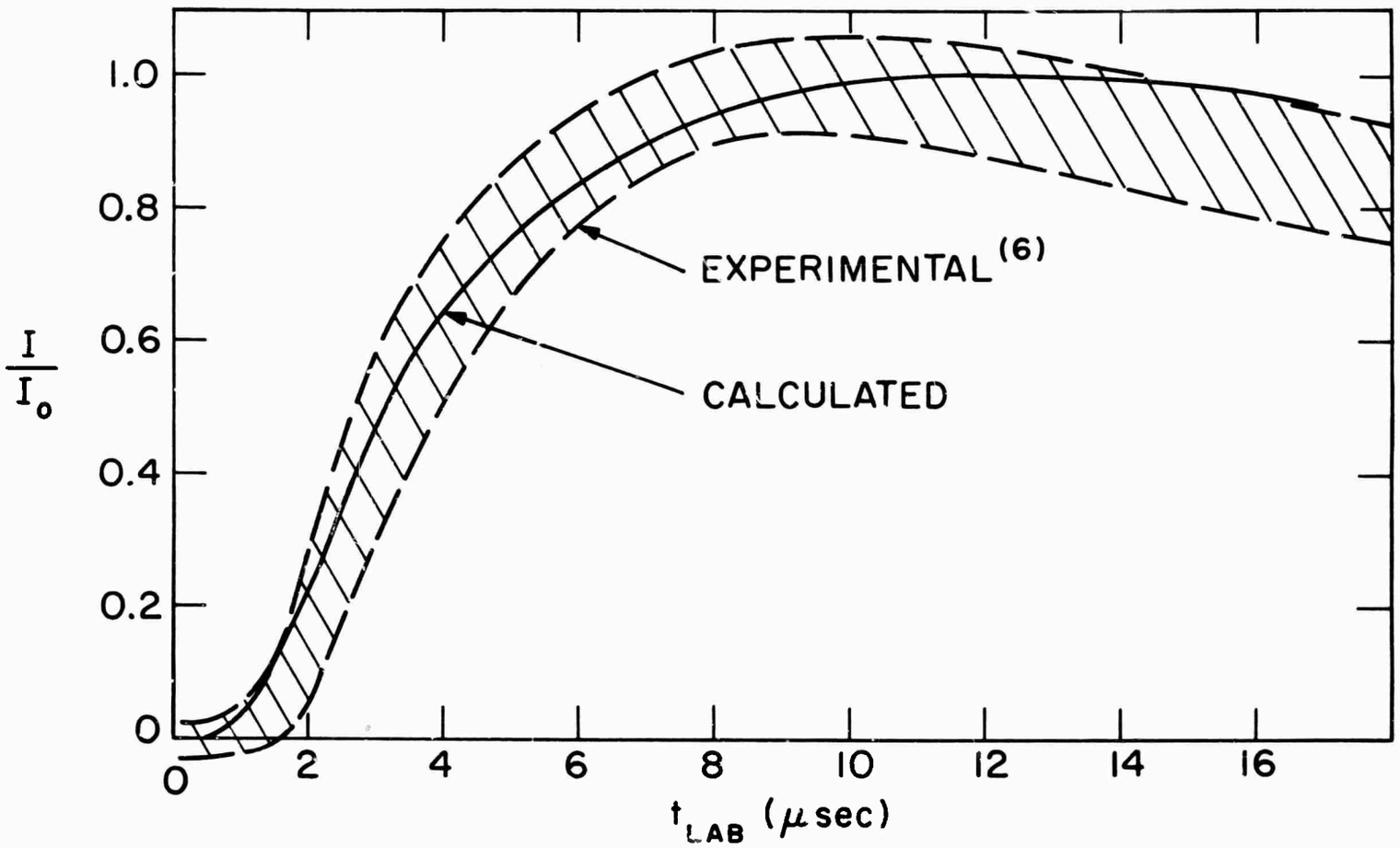
1.0
0.8
0.6
0.4
0.2
0
$\frac{I}{I_o}$
0
2
4
6
8
10
12
14
16
t_{LAB} (μsec)
EXPERIMENTAL (6)
CALCULATED

FIGURE 9